LSTM-Based Facial Performance Capture Using Embedding Between Expressions*

Hsien-Yu Meng†
Owlii
Beijing, China 100084
xianyu.meng@owlii.com

Tzu-Heng Lin
Owlii
Beijing, China 100084
ziheng.lin@owlii.com

Xiubao Jiang
Owlii
Beijing, China 100084
xiubao.jiang@owlii.com

Yao Lu
Owlii
Beijing, China 100084
yao.lu@owlii.com

Jiangtao Wen
Tsinghua University
Beijing, China 100084
jiangtaowen.wen@gmail.com

ABSTRACT

We present a novel end-to-end framework for facial performance capture given a monocular video of an actor's face. Our framework are comprised of 2 parts. First, to extract the information in the frames, we optimize a triplet loss to learn the embedding space which ensures the semantically closer facial expressions are closer in the embedding space and the model can be transferred to distinguish the expressions that are not presented in the training dataset. Second, the embeddings are fed into an LSTM network to learn the deformation between frames. In the experiments, we demonstrated that compared to other methods, our method can distinguish the delicate motion around lips and significantly reduce jitters between the tracked meshes.

CCS CONCEPTS

• **Computing methodologies** → **Neural networks**; **Animation**; **Motion capture**;

KEYWORDS

Facial Animation, Transfer Learning, Facial Performance Capture

ACM Reference format:
Hsien-Yu Meng, Tzu-Heng Lin, Xiubao Jiang, Yao Lu, and Jiangtao Wen. 2018. LSTM-Based Facial Performance Capture Using Embedding Between Expressions. In *Proceedings of ACM SIGGRAPH / Eurographics Symposium on Computer Animation, Paris, France, July 2018 (SCA'18),* 8 pages.
DOI: 10.1145/nnnnnnn.nnnnnnn

1 INTRODUCTION

In feature films and video games, digital characters are prominent, and it is crucial to delivering accurate facial animation since human is sensitive to delicate and slight facial motions such as compressed lips, stretched lips, pucker and dimple. Conventional facial animation pipelines require manual correction and removing artifacts to ensure that lip and eye contours are natural, and it requires tremendous efforts when there are several hours-long footages to be processed.

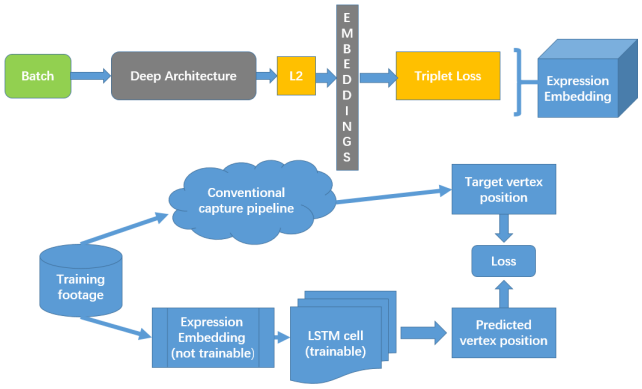

Figure 1: Capture Pipeline

In this paper, we present a transfer learning method to train an expression classifier with 23 basic expressions, and the trained model can be used to distinguish different expressions that do not appear in the training set with Euclidean distance. From the trained model, an expression embedding space can be constructed. For an input video footage, it can be mapped into this space and the embeddings are fed into an LSTM network, which will generate the blend shape coefficients. Our end-to-end framework takes in a 10 minutes' single view RGBD video footage [Weise et al., 2009] as training input, and after training it can process the remaining video footage at 137 FPS on our server. Figure 1 illustrates the general pipeline of our framework. Furthermore, compared to other deep-learning method proposed in [Laine et al., 2016] and [Cao et al., 2014a], our expression embedding space can incorporate more delicate motion around eyes and lips, and our LSTM network can encode the time-related features to significantly reduce jitters between meshes as illustrated in Figure 12 and Figure 11.

The rest of this paper is organized as following: Section 2 introduces related works in facial expression capture field; Section 3

*Produces the permission block, and copyright information
†

SCA'18, Paris, France

DOI: 10.1145/nnnnnnn.nnnnnnn

defined the architecture of our network while Section 4 describes how we choose the baseline and setup the experiment and compares the result of our design and the baseline; Section 5 sums up the whole paper.

2 RELATED WORK

Conventional approaches to capturing highly detailed facial expressions can be divided into two divisions. The first one requires depth information, either from multi-view videos [Beeler et al., 2011][Fyffe et al., 2011][Ghosh et al., 2011] or from structural light [Zhang and Huang, 2004][Li et al., 2009] as Digital Emily Project proposed by [Alexander et al., 2010].

The second kind requires no depth information but explores other information to capture the facial expression. In the production-level environment, marker-based techniques with manually drawn contours over the lip and eye regions on RGB image to ensure accurate lip and eye contour [Bhat et al., 2013] are widely used. However, in real-time face capture, markless techniques are more common, which rely on texture information [Thies et al., 2016][Romdhani and Vetter, 2005] to generate the PCA coefficients of vertices and textures. It generally requires a well-collected face dataset including meshes and textures of different identities and construct PCA base vectors. An energy function is designed and by minimizing it we get the best PCA coefficients. Moreover, the method proposed in [Thies et al., 2016] employs Gaussian-Newton algorithm to minimize the difference between the input image and rendered one, which requires rendering the generated mesh and computing the derivatives of cost function respect to every PCA coefficients at each iteration. While the texture generated from PCA basis is not realistic enough, to improve this, [Saito et al., 2016] proposed a deep learning method to synthesize the texture.

Eigenfaces proposed by [Turk and Pentland, 1991] represent facial appearances as linear models and several works were proposed to extend it [Booth et al., 2016][Donner et al., 2006][Matthews and Baker, 2004]. The multi-linear PCA model can be described as below:

$$M_{geo}(\alpha, \delta) = a_{id} + E_{id} \cdot \alpha + E_{exp} \cdot \delta \tag{1}$$

$$M_{alb}(\beta) = a_{alb} + E_{alb} \cdot \beta \tag{2}$$

where a_{id} is the average shape, a_{alb} is the average reflectance, Eid is basis of shape, E_{exp} is basis of expression and E_{alb} is basis of reflectance. Basically α and β are the parameters in optimization problems.

Another approach to capturing the distinctive expression of an actor is designated blendshape rigs. The mesh can be described as below:

$$M_{geo}(\alpha) = B_0 + \Sigma_{i=1}^{N} \alpha_i \cdot (B_i - B_0) \tag{3}$$

where N is number of blendshapes excluding the neutral blendshape, B_0 is the neutral expression and α is the coefficients to be applied to B_i. Blendshape makes it easier for CG system to transfer the controller semantics and expression dynamics from a generic template to the target blendshape model mentioned in [Li et al., 2010].

Figure 2: Part of FaceWarehouse dataset, each column are labeled the same

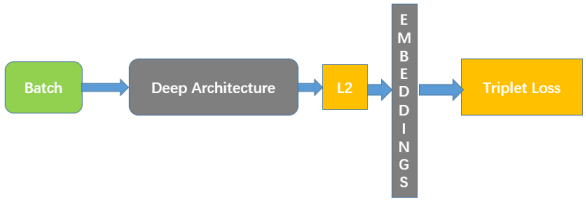

Figure 3: FaceNet Model proposed in [Schroff et al., 2015]

3 NETWORK ARCHITECTURE

Our network contains 2 networks. The first one is FaceNet [Schroff et al., 2015] optimized with triplet loss to perform expression verification and extract embeddings from the input video footage. The second one is an LSTM-based network which takes in a sequence of embedding vectors generated by the optimized FaceNet and attempts to learn the deformation between the embeddings as well as the mapping function between embeddings and blendshape coefficients.

Our training dataset is comprised of 2 datasets. The FaceWarehouse dataset is composed of 150 persons with 23 different facial expressions as illustrated in Figure 2. And the input footage is consist of 3500 frames at 30 FPS. Our target output is 51 coefficients of blendshapes, which are the combinations of different expression of an actor such as mouth press, mouth stretch, and mouth smile, etc. Every blendshape contains 7366 vertices and 14600 triangles.

3.1 Expression Embedding

FaceNet [Schroff et al., 2015] is a popular network for face verification problems. It maps the face images to embedding space where Euclidean distance represents the similarity of faces as demonstrated in Figure 4. By optimizing the triplet loss $L(anchor, positive, negative)$, it minimizes $||anchor-positive||_2^2$, and maximize $||anchor-negative||_2^2$.

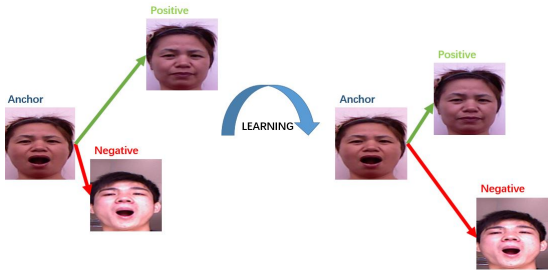

Figure 4: Triplet Loss in face verification problems : the anchor and the positive samples are same people while the anchor and the negative samples are different people

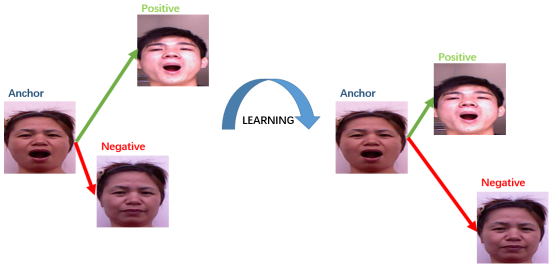

Figure 5: Triplet Loss in our experiment : the anchor and the positive samples are semantically same expression while the anchor and the negative samples are semantically different expression

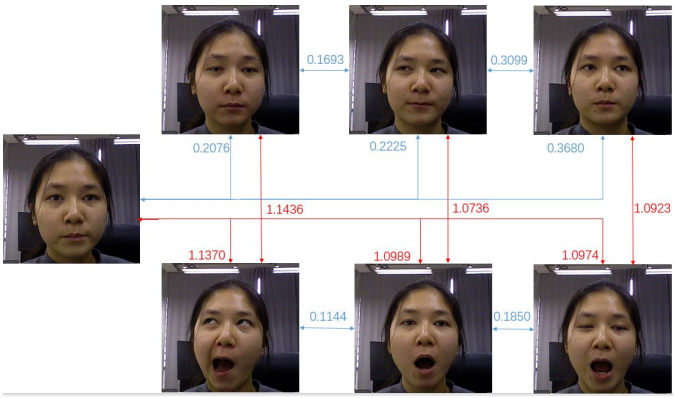

Figure 6: L2-norm between embeddings of frames on evaluation dataset

Figure 3 shows its architecture while Table 1 lists the detailed parameters. The goal is to ensure that in the embedding space, an image $x_i^a(anchor)$ of a specific expression is closer to those $x_i^p(positive)$ of the same expression than those $x_i^n(negative)$ of different expression, as illustrated in Figure 5. The Loss function L is defined as:

$$\Sigma_i^N[||f(x_i^a) - f(x_i^p)||_2^2 - ||f(x_i^a) - f(x_i^n)||_2^2|| + \alpha] \quad (4)$$

where α is a margin that is enforced between positive and negative pairs and N is the cardinality of all possible triplets in training set.

Table 1: FaceNet Architecture [Schroff et al., 2015]

Name	kernel	stride	input-channels	output-channels	activation
conv1	7x7	2	3	64	ReLU
pool1	3x3	2	64	64	
rnorm1					
conv2a	1x1	1	64	64	ReLU
conv2	3x3	1	64	192	ReLU
rnorm2					
pool2	3x3	2	192	192	
conv3a	1x1	1	192	192	
conv3	3x3	1	192	384	
pool3	3x3	2	384	384	
conv4a	1x1	1	384	384	ReLU
conv4	3x3	1	384	256	ReLU
conv5a	1x1	1	256	256	ReLU
conv5	3x3	1	256	256	ReLU
conv6a	1x1	1	256	256	ReLU
conv6	3x3	1	256	256	ReLU
pool4	3x3	2	256	256	
concat					
fc1				128	
fc2				128	

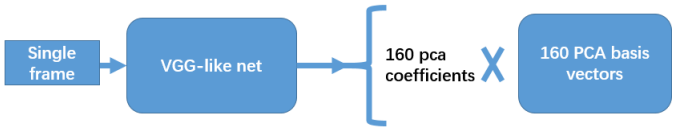

Figure 7: VGG-like framework [Laine et al., 2016]

3.2 LSTM Network

After FaceNet is trained and tuned on FaceWarehouse dataset, the model is applied to infer the embedding of frames of a monocular video. We build a sequence LSTM network of length 10, the hidden state is set to 1×256 and each cell output 51 coefficients for corresponding blendshapes. The LSTM network architecture is shown in Figure 7. The hidden state is sent to the next cell so that the network can learn the deformation between embeddings.

To examine whether the embedding carries enough information from frames for our LSTM network, we did two experiments as shown in Figure 8.

First, we implement the end-to-end VGG-like framework mentioned in [Laine et al., 2016]. Figure 7 shows the architecture of the network and Table 2 lists the detailed parameters.

Second, we build a deep network similar to the network proposed in [Laine et al., 2016], feed the fully connected layer's output into LSTM network and train them together as the baseline. Furthermore, by changing the kernel size in *conv_a* layers to 1x1, we only change the dimension in filter space. At the pre-processing step, we do not calculate the mean and variance across all training images to whiten the training set. The two networks are illustrated in Table 2 and Table 3. In the first comparison experiments, we do PCA analysis on all training meshes and choose 160 basis vectors, which can

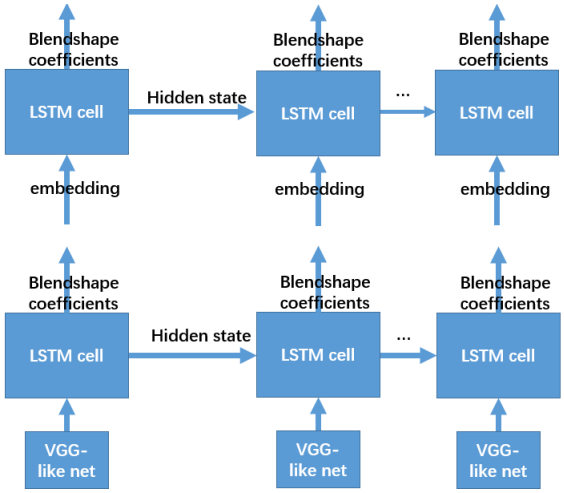

Figure 8: Experiment: the first row is our pretrained FaceNet + LSTM network, the second row is the VGG-like network trained with LSTM network

Table 2: Network Architecture in [Laine et al., 2016]

Name	kernel	stride	input-channels
conv1a	3x3	2	1
conv1b	3x3	1	64
conv2a	3x3	2	64
conv2b	3x3	1	96
conv3a	3x3	2	96
conv3b	3x3	1	144
conv4a	3x3	2	144
conv4b	3x3	1	216
conv5a	3x3	2	216
conv5b	3x3	1	324
conv6a	3x3	2	324
conv6b	3x3	1	486
drop			
fc			
fc			

Table 3: Network Architecture in Our experiments

Name	kernel	stride	input-channels	output-channels	activation
conv1a	1x1	2	3	64	ReLU
conv1b	3x3	1	64	64	ReLU
conv2a	1x1	2	64	96	ReLU
conv2b	3x3	1	96	96	ReLU
conv3a	1x1	2	96	144	ReLU
conv3b	3x3	1	144	144	ReLU
conv4a	1x1	2	144	216	ReLU
conv4b	3x3	1	216	216	ReLU
conv5a	1x1	2	216	324	ReLU
conv5b	3x3	1	324	324	ReLU
conv6a	1x1	2	324	486	ReLU
conv6b	3x3	1	486	486	ReLU
drop					
fc				160	linear
fc				PCA_num	linear

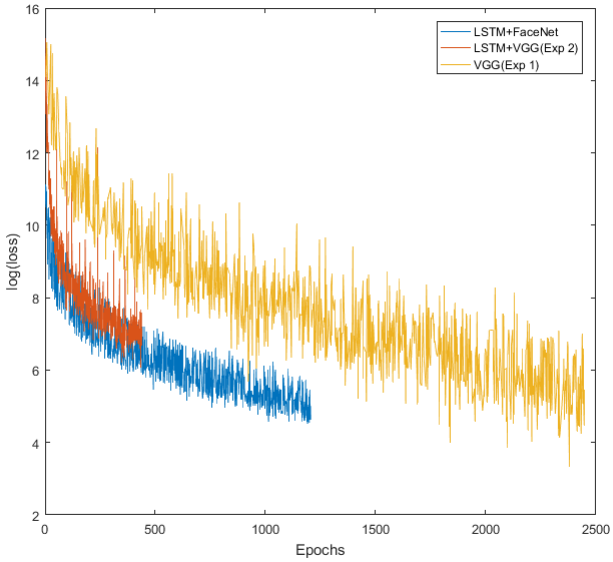

Figure 9: log *Loss* **: the blue line is the training loss of pre-trained FaceNet + LSTM network, the red line is the training loss of the VGG-like network trained with LSTM network, the orange line is the network mentioned in [Laine 2017] [Laine et al., 2016].**

explain 99.9% variances in the training set. The loss-vs-epochs of 3 networks are shown in Figure 9. We sum up all squared difference between meshes predicted by LSTM network and ground truth meshes as the loss.

4 EXPERIMENTS

4.1 Expression Embedding

We aim to train the network to extract the good features of footage images. In the experiment, we use the FaceWarehouse [Cao et al., 2014b] dataset for training as demonstrated in Figure 2, which contains frontal images of 150 persons and each person's 23 different expressions. Furthermore, the semantically same expressions are labelled same thus there are 23 labels in our training set. In the training, we randomly sample the negative and positive training examples and feed them to the deep architecture to acquire the embeddings of those examples.

In the training step, the FaceWarehouse dataset is cropped and resized into 160×160, the batch size is set to 24 and the loss became 1/125 of original loss after 375k epochs using 3 GeForce GTX 1080 cards. In the evaluation step, we generated expression embeddings from pre-trained model mentioned above and calculate the L2-norm between semantically different expressions.

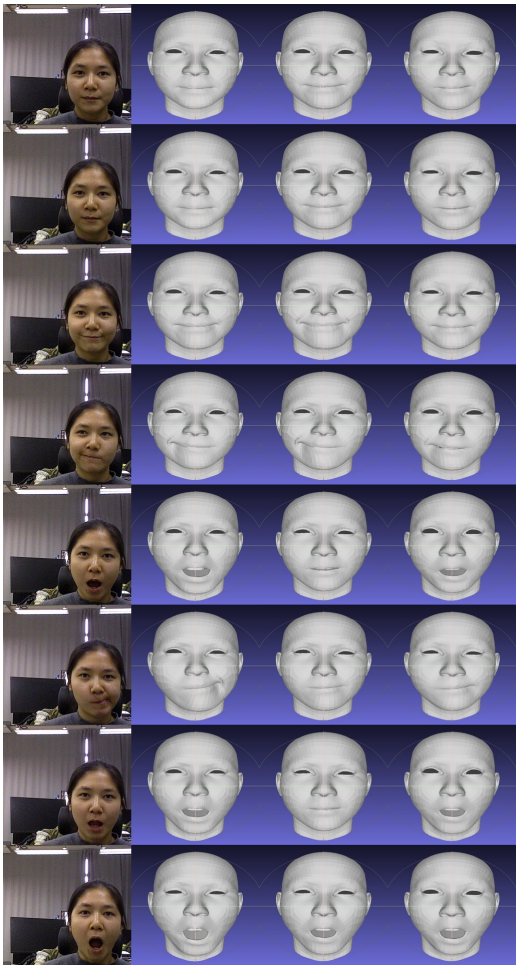

Figure 10: Comparison : the first column is the footage, the second column is ground truth, the third column is result of VGG-like network as Figure 7 described in [Laine 2017][Laine et al., 2016], the fourth column is the result of our network.

The result inferred from evaluation dataset is shown in Figure 6 and it indicates that the L2-norm between neutral expressions is smaller than the L2-norm between the mouth-open expressions. Note that the pre-trained model is trained on FaceWarehouse dataset and evaluated on another footage, therefore, we can safely draw the conclution that the model is not over-fitting although the training set contains only 3450 images.

4.2 Comparison

Since the LSTM network can capture the time-related features and reduce the jitters between meshes, we visualize the result of our network in comparison with the baseline VGG-like network.

Figure 11, Figure 12, Figure 13 and Figure 14 are the results of 5 continuous frames in the validation video footage. The first row shows our result while the second row shows the result of the baseline VGG-like network.

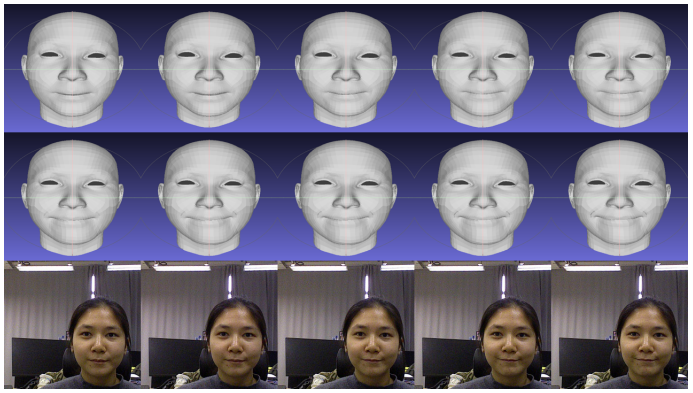

Figure 11: Neutral Expression to Smile. The first row is our result; the second row is result of VGG-like network as Figure7 described in [Laine 2017][Laine et al., 2016]. See Figure 15 for numerical analysis

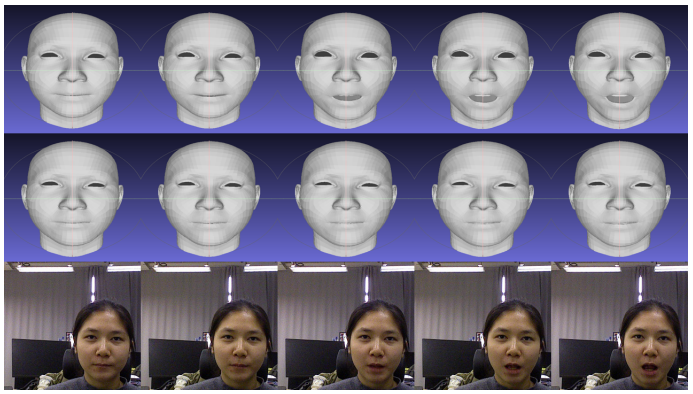

Figure 12: Neutral Expression to Mouth-Open Expression. The first row is our result; the second row is result of VGG-like network as Figure7 described in [Laine 2017][Laine et al., 2016]. See Figure 16 for numerical analysis

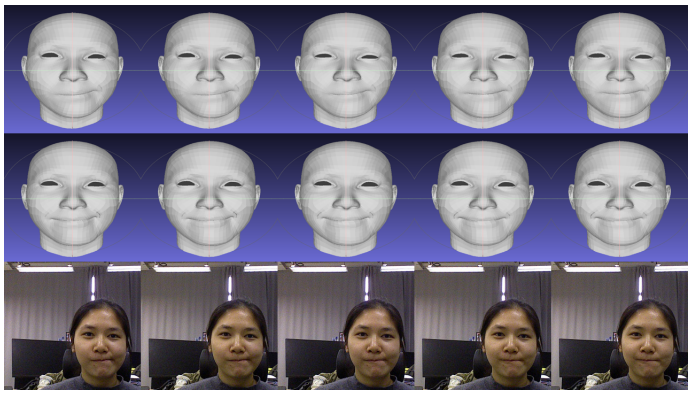

Figure 13: Mouth-Press-Left Expression to Compressed-Lips Expression. The first row is our result; the second row is result of VGG-like network as Figure7 described in [Laine 2017][Laine et al., 2016]

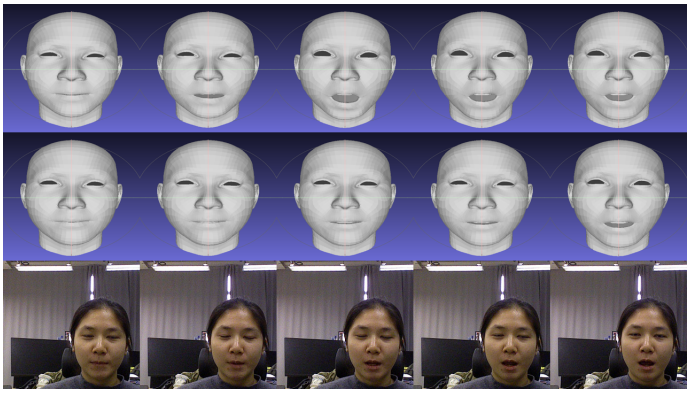

Figure 14: Failure Case : Neutral Expression to Mouth-Open Expression. The first row is our result; the second row is result of VGG-like network as Figure7 described in [Laine 2017][Laine et al., 2016]

As an example, Figure 11 illustrates the deformation from a neutral expression to smile expression, and notice that the baseline (second row) is almost the same within the 5 continuous frames while our result (first row) shows more delicate deform process in lip region and eye region, as the eye region is getting smaller when the actor is smiling.

To represent a quantified measurement of jitters between frames, we define the mean squared difference D between frame $f-1$ and frame f as described below:

$$D^{\{f\}} = \frac{1}{N}\Sigma_i^N \sqrt{||v_i^{\{f-1\}} - v_i^{\{f\}}||_2^2} \tag{5}$$

where f is the frame index in the footage video and N is number of vertices of mesh.

Figure 15 illustrates D of frames when the actor is changing from a neutral expression to smile expression. The baseline (VGG) shows a high peak at frame 2, which represents a sudden change in the reconstructed expression. This kind of jitters is common in the baseline's result. However, our result has a steadier D, which suggests that the reconstructed expression is changing more smoothly.

Figure 16 illustrates D between frames in Figure 12. When $f = 3$ the actor's mouth is open, and $D^{\{3\}}$ is supposed to be the highest value among $\{D^{\{1\}}, D^{\{2\}}, ..., D^{\{5\}}\}$. We can notice that the baseline (VGG) is much lower than our result (LSTM+FaceNet), which indicates the expression reconstructed by the baseline has smaller motion. This verifies what we have observed in the comparison between the first and the second row in Figure 12.

Figure 17 and Figure 18 show the comparison between our result and the result of conventional method proposed by [Cao et al., 2014a], which generates the next frame based on the the α mentioned in Eq.1 and displacement coefficients of current frame.

Compared Figure 11 to Figure 13, it is clear that the VGG-like network cannot distinguish the intrinsic motion around lips while ours can.

Figure 14 shows a failure case, which contains 5 continuous frames from a neutral expression to mouth-open expression. The

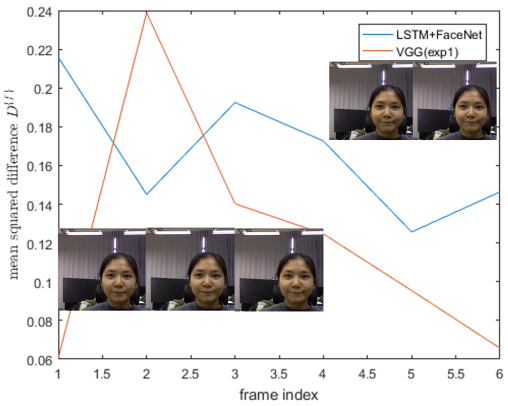

Figure 15: mean squared difference analysis of Figure11 defined in Eq.5

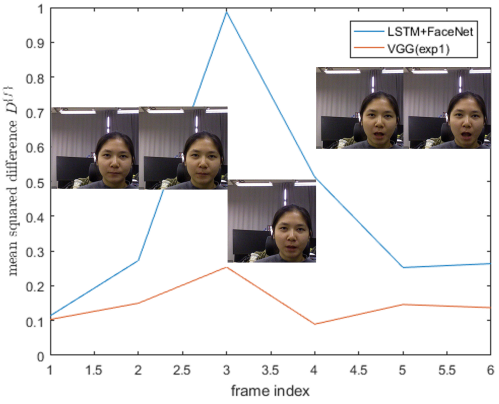

Figure 16: Mean squared difference analysis of Figure 12 defined in Eq.5

first row in Figure 14 demonstrates a motion from neutral to mouth-open-large expression and then to mouth-open-small expression while the second row demonstrates a motion from a neutral expression to mouth-open-small expression. To claim this issue, we visualize the L2-norm between frames in Figure 19. The elements on diagonal have a value of zero, which is as expected. However, notice that element $(2, 3)$ has almost the same value as element $(2, 4)$, which suggests that the expression embedding space is not trained well as the L2-norm cannot reflect the degree of mouth-opening. This can explain the failure case in Figure 14.

5 CONCLUSION

Figure 10 illustrates the comparison of ground-truth, VGG-like network [Laine et al., 2016] and our result, which suggests that the VGG-like network cannot discriminate the mouth-open-like expressions such as mouth-open-right and mouth-open-left. Moreover, Figure 13 suggests that the model can be transferred to distinguish the delicate lip expressions (mouth-press-left and compressed-lips) which do not appear in the training dataset. For LSTM network,

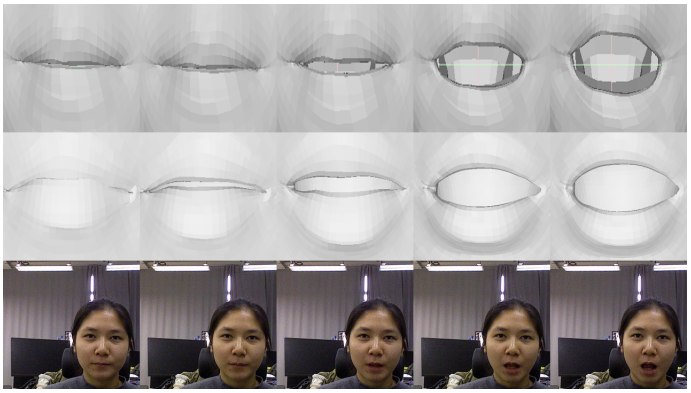

Figure 17: Comparison : Neutral Expression to Mouth-Open Expression. The first row is our result; the second row is result of DDE proposed by [Cao 2014] [Cao et al., 2014a]

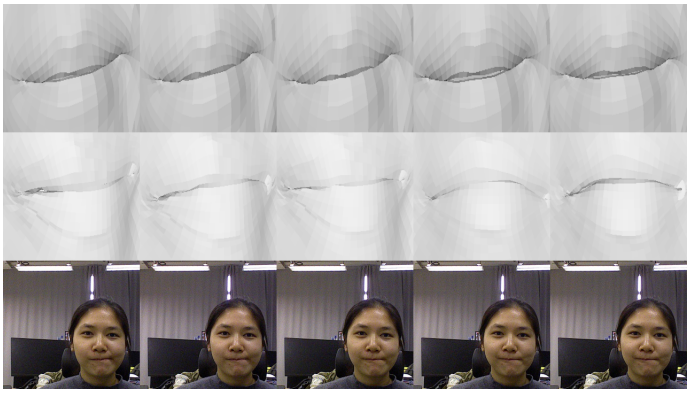

Figure 18: Comparison : Mouth-Press-Left Expression to Compressed-Lips Expression. The first row is our result; the second row is result of DDE proposed by [Cao 2014] [Cao et al., 2014a]

we claim that this network can learn the deformation between embeddings and perform more smooth result as demonstrated in Figure 11 and Figure 13.

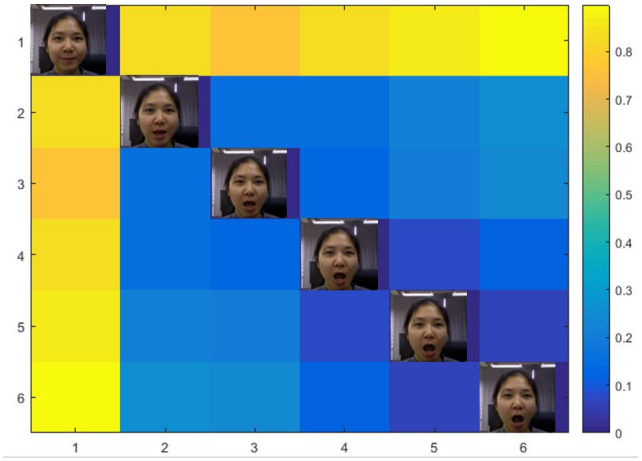

Figure 19: Heatmap of L2-norm between neutral expression and mouth-open expressions on diagonal

REFERENCES

2016 IEEE Conference on Computer Vision and Pattern Recognition, CVPR 2016, Las Vegas, NV, USA, June 27-30, 2016, 2016. IEEE Computer Society. ISBN 978-1-4673-8851-1. URL http://ieeexplore.ieee.org/xpl/mostRecentIssue.jsp?punumber=7776647.

O. Alexander, M. Rogers, W. Lambeth, J. Chiang, W. Ma, C. Wang, and P. E. Debevec. The digital emily project: Achieving a photorealistic digital actor. *IEEE Computer Graphics and Applications*, 30(4):20–31, 2010. doi: 10.1109/MCG.2010.65. URL https://doi.org/10.1109/MCG.2010.65.

T. Beeler, F. Hahn, D. Bradley, B. Bickel, P. A. Beardsley, C. Gotsman, R. W. Sumner, and M. H. Gross. High-quality passive facial performance capture using anchor frames. *ACM Trans. Graph.*, 30(4):75:1–75:10, 2011. doi: 10.1145/2010324.1964970. URL http://doi.acm.org/10.1145/2010324.1964970.

K. S. Bhat, R. Goldenthal, Y. Ye, R. Mallet, and M. Koperwas. High fidelity facial animation capture and retargeting with contours. In *The ACM SIGGRAPH / Eurographics Symposium on Computer Animation, SCA '13, Anaheim, CA, USA, July 19-21, 2013*, pages 7–14, 2013. doi: 10.1145/2485895.2485915. URL http://doi.acm.org/10.1145/2485895.2485915.

J. Booth, A. Roussos, S. Zafeiriou, A. Ponniah, and D. Dunaway. A 3d morphable model learnt from 10, 000 faces. In *2016 IEEE Conference on Computer Vision and Pattern Recognition, CVPR 2016, Las Vegas, NV, USA, June 27-30, 2016* DBL [2016], pages 5543–5552. ISBN 978-1-4673-8851-1. doi: 10.1109/CVPR.2016.598. URL https://doi.org/10.1109/CVPR.2016.598.

C. Cao, Q. Hou, and K. Zhou. Displaced dynamic expression regression for real-time facial tracking and animation. *ACM Trans. Graph.*, 33(4):43:1–43:10, 2014a. doi: 10.1145/2601097.2601204. URL http://doi.acm.org/10.1145/2601097.2601204.

C. Cao, Y. Weng, S. Zhou, Y. Tong, and K. Zhou. Facewarehouse: A 3d facial expression database for visual computing. *IEEE Trans. Vis. Comput. Graph.*, 20(3):413–425, 2014b. doi: 10.1109/TVCG.2013.249. URL https://doi.org/10.1109/TVCG.2013.249.

R. Donner, M. Reiter, G. Langs, P. Peloschek, and H. Bischof. Fast active appearance model search using canonical correlation analysis. *IEEE Trans. Pattern Anal. Mach. Intell.*, 28(10):1690–1694, 2006. doi: 10.1109/TPAMI.2006.206. URL https://doi.org/10.1109/TPAMI.2006.206.

G. Fyffe, T. Hawkins, C. Watts, W. Ma, and P. E. Debevec. Comprehensive facial performance capture. *Comput. Graph. Forum*, 30(2):425–434, 2011. doi: 10.1111/j.1467-8659.2011.01888.x. URL https://doi.org/10.1111/j.1467-8659.2011.01888.x.

A. Ghosh, G. Fyffe, B. Tunwattanapong, J. Busch, X. Yu, and P. E. Debevec. Multiview face capture using polarized spherical gradient illumination. *ACM Trans. Graph.*, 30(6):129:1–129:10, 2011. doi: 10.1145/2070781.2024163. URL http://doi.acm.org/10.1145/2070781.2024163.

S. Laine, T. Karras, T. Aila, A. Herva, and J. Lehtinen. Facial performance capture with deep neural networks. *CoRR*, abs/1609.06536, 2016. URL http://arxiv.org/abs/1609.06536.

H. Li, B. Adams, L. J. Guibas, and M. Pauly. Robust single-view geometry and motion reconstruction. *ACM Trans. Graph.*, 28(5):175:1–175:10, 2009. doi: 10.1145/1618452.1618521. URL http://doi.acm.org/10.1145/1618452.1618521.

H. Li, T. Weise, and M. Pauly. Example-based facial rigging. *ACM Trans. Graph.*, 29(4):32:1–32:6, 2010. doi: 10.1145/1833351.1778769. URL http://doi.acm.org/10.1145/1833351.1778769.

I. A. Matthews and S. Baker. Active appearance models revisited. *International Journal of Computer Vision*, 60(2):135–164, 2004. doi: 10.1023/B:VISI.0000029666.37597.d3. URL https://doi.org/10.1023/B:VISI.0000029666.37597.d3.

S. Romdhani and T. Vetter. Estimating 3d shape and texture using pixel intensity, edges, specular highlights, texture constraints and a prior. In *2005 IEEE Computer Society Conference on Computer Vision and Pattern Recognition (CVPR 2005), 20-26 June 2005, San Diego, CA, USA*, pages 986–993, 2005. doi: 10.1109/CVPR.2005.145. URL https://doi.org/10.1109/CVPR.2005.145.

S. Saito, L. Wei, L. Hu, K. Nagano, and H. Li. Photorealistic facial texture inference using deep neural networks. *CoRR*, abs/1612.00523, 2016. URL http://arxiv.org/abs/1612.00523.

F. Schroff, D. Kalenichenko, and J. Philbin. Facenet: A unified embedding for face recognition and clustering. *CoRR*, abs/1503.03832, 2015. URL http://arxiv.org/abs/1503.03832.

J. Thies, M. Zollhöfer, M. Stamminger, C. Theobalt, and M. Nießner. Face2face: Real-time face capture and reenactment of RGB videos. In *2016 IEEE Conference on Computer Vision and Pattern Recognition, CVPR 2016, Las Vegas, NV, USA, June 27-30, 2016* DBL [2016], pages 2387–2395. ISBN 978-1-4673-8851-1. doi: 10.1109/CVPR.2016.262. URL https://doi.org/10.1109/CVPR.2016.262.

M. Turk and A. Pentland. Eigenfaces for recognition. *J. Cognitive Neuroscience*, 3(1):71–86, Jan. 1991. ISSN 0898-929X. doi: 10.1162/jocn.1991.3.1.71. URL http://dx.doi.org/10.1162/jocn.1991.3.1.71.

T. Weise, H. Li, L. J. V. Gool, and M. Pauly. Face/off: live facial puppetry. In *Proceedings of the 2009 ACM SIGGRAPH/Eurographics Symposium on Computer Animation, SCA 2009, New Orleans, Louisiana, USA, August 1-2, 2009*, pages 7–16, 2009. doi: 10.1145/1599470.1599472. URL http://doi.acm.org/10.1145/1599470.1599472.

S. Zhang and P. Huang. High-resolution, real-time 3d shape acquisition. In *2004 Conference on Computer Vision and Pattern Recognition Workshop*, pages 28–28, June 2004. doi: 10.1109/CVPR.2004.86.